

Eddy current coil interaction with a right-angled conductive wedge

BY T. P. THEODOULIDIS¹ AND J. R. BOWLER²

¹*Department of Engineering and Management of Energy Resources, University of West Macedonia, Kastorias and Fleming, 50100 Kozani, Greece*
(theodoul@ieee.org)

²*Center for Nondestructive Evaluation, Iowa State University, Applied Sciences Complex II, 1915 Scholl Road, Ames, IA 50011, USA*
(jbowler@iastate.edu)

The time-harmonic electromagnetic field in an electrically conductive right-angled wedge due to an inductive excitation by circular coil in air has been calculated. Using a formulation in Cartesian coordinates, the problem domain is truncated in a dimension whose axis is normal to a wedge face, and an approximate series solution found using elementary functions satisfying Maxwell's equations in the quasi-static limit. The coil impedance variation with position and frequency is calculated and compared with measurements made on a coil near the edge of a large aluminium block which approximates the effect of a conductive quarter-space. The comparison between theory and experiment shows very close agreement.

Keywords: eddy current; conductive wedge; coil impedance

1. Introduction

The quasi-static electromagnetic field in a conductive wedge has been determined for the case where the excitation is an alternating current in a coil whose axis is normal to one of the wedge faces. The problem has applications in eddy current non-destructive evaluation (NDE) and its solution completes a preliminary stage in a larger task to determine the eddy current probe response due to a corner crack in a metal. In order to find the field in a homogeneous conductive quarter space due to an external inductive excitation at an arbitrary frequency, we are obliged to find a solution to a penetrable wedge problem. In the theory of wave diffraction and diffusion between adjoining regions having different material properties, a crucial step is to match solutions at the interfaces. In the case of wedged shaped regions, exact closed form solutions have not been found due to the formidable difficulties of matching the field across the boundaries between the different media. However, a number of approaches have been used to find approximate solutions. In particular, [Budaev \(1995\)](#) has discussed the Sommerfeld–Maliuzhinetz formulation of the penetrable wedge problem in elastodynamics and suggested a method for finding approximate solutions. In contrast [Rawlins \(1999\)](#) used the Kontorovich–Lebedev transform to derive a

solution for a penetrable dielectric wedge using perturbation methods assuming a low contrast between adjoining media. Although the corresponding eddy current problem could be approached using perturbation theory for the thin skin or large skin depth regimes, we have sought instead a method that can be applied for a wide frequency range while ensuring the correct continuity of the field at conductor–air interfaces.

For a half-space conductor, which like the quarter space can be viewed as a special case of a wedge problem, closed form integral expressions for the electromagnetic field are easily derived for a coil whose axis is normal to the surface. Similar solutions for a stratified half-space (Dodd & Deeds 1968) have been widely used for applications in NDE, see Tai *et al.* (2002) and references therein. Eddy current probes typically have ferrite cores but the problem of calculating the core magnetization need not defeat the determined analyst. An approximate solution has been found for a normal coil with a cylindrical coaxial ferrite core of finite length, despite the added complexity of dealing with extra interface conditions at the core–air interface (Theodoulidis 2003). The electric field of the probe has been found by truncating the domain of the problem to one of finite radius and expressing the solution as a series. In this way the task of satisfying the boundary conditions is made tractable. Here we extend this strategy to a conductive wedge problem with a coil excitation. What we call the ‘truncated region eigenfunction expansion’ (TREE) method has been used to find an approximate match between the electromagnetic field in air and the field in a conductive quarter space.

Domain truncation is typically applied to a domain dimension that is infinite according to the original problem definition. Limits are imposed in the infinite spatial dimension by adding artificial boundaries and forcing the solution to be zero there. This procedure gives rise to errors but these errors can be made as small as desired by adjusting the location of the imposed boundaries to make them more remote from the field source. The solution in the truncated dimension can be written as a series expansion of eigenfunctions rather than as an integral. Computations then are carried out by limiting the number of terms in the series. Although the series truncation gives rise to a further source of error, this error is also easily controlled.

In solving a complicated boundary value problem, it may be necessary, as here, to subdivide the domain of the problem, construct a formal solution for each region and use interface conditions to match the sub-domain solutions across their boundaries. With sub-domain solutions in the form of series expansions, it is convenient to represent the expansion coefficients as column vectors related to one another through the interface conditions. The relationships take the form of simultaneous matrix equations for the coefficient vectors. In the TREE method, these matrix equations are then solved to get the expansion coefficients in terms of a prescribed source-field column vector. Computation of the solution coefficient vector is done numerically, hence the method can be considered semi-analytical. However, the essential point is that the solution has an analytical form that satisfies the governing equations, although the boundary conditions are satisfied only approximately. The scheme can be applied to a number of configurations (Theodoulidis 2003, 2004). Here it is used to find an approximate solution of a penetrable wedge problem using elementary functions.

The problem is formulated in terms of a transverse electric (TE) and a transverse magnetic (TM) scalar potential. As a first step in the solution, a

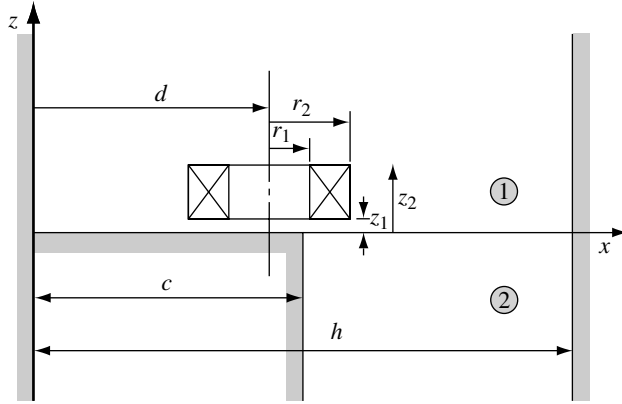


Figure 1. Coil in the presence of a conductive quarter space.

column vector representing the coefficients of the eigenfunction expansion of the TE potential in the absence of the conductor is determined. This is the prescribed source column vector. Then the corner conductor is introduced, series solutions are constructed for each sub-region of the problem and matched across the boundaries. Finally, the unknown coefficient vectors are expressed in terms of the source vector and an equation for the coil impedance is derived.

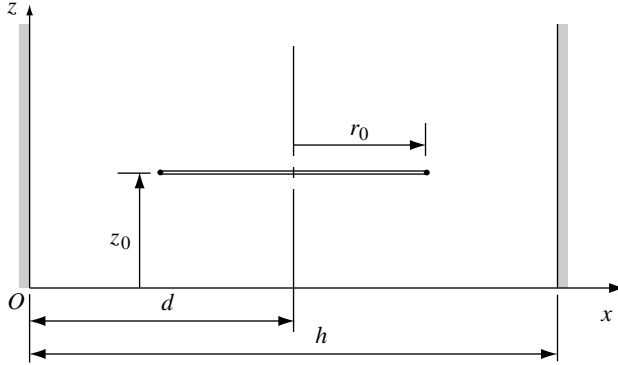
2. Scalar decomposition

A time-harmonic magnetic flux density, varying at an angular frequency ω as the real part of $\exp(j\omega t)$, is here expressed in terms of second order potentials

$$\mathbf{B} = \nabla \times \nabla \times \mathbf{W} \quad \text{with} \quad \mathbf{W} = \hat{x} W_a + \hat{x} \times \nabla W_b. \quad (2.1)$$

The potentials, W_a and W_b , are sought for the quasi-static field of a circular coil whose axis is normal to one of the faces of a conductive quarter space, [figure 1](#). The coil axis is in the z -direction and the outward normals to the faces of the conductor are in the z - and x -directions. Because the potentials are defined with respect to the x -direction, they are coupled through the interface conditions at the conductor–air interface whose normal is z -directed. It may seem that at the other interface, there is no coupling between potentials but in fact we find that there is. The challenge of the quarter space problem is to satisfy the interface conditions simultaneously.

A formal solution can be established by Fourier transformation of the field in the x - and y -directions. In the approach chosen, the domain of the problem is restricted in the x -direction to a region between $x=0$ and $x=h$. On the boundaries formed by the domain truncation, the normal component of the magnetic flux density is set to zero. A Fourier integral representation is used for the y -dependence whereas the x -dependence of the field is expressed as a Fourier series. Truncation of the series leads to an approximation of the unbounded domain solution but the errors introduced can be made as small as desired by increasing the width of the domain.

Figure 2. Circular filamentary coil in the plane $z=z_0$.

The first stage of the process is to derive an expression for the coil field in a form that can be used subsequently to solve the corner conductor problem. This means that the TE potential W_a , defined with respect to the x -direction, must be found for a coil in free space whose axis is in the z -direction. The result is expressed as a superposition of eigenfunctions whose coefficients form the predefined source vector for the corner problem.

3. Coil field

(a) Circular filament in free space

Consider a circular current filament of radius r_0 in the plane $z=z_0$ whose axis is parallel to and at a distance d from the z -axis, [figure 2](#). The magnetic flux density due to the filament is written in terms of the TE potential

$$\mathbf{B} = \nabla \left(\frac{\partial W_a^{(0)}}{\partial x} \right). \quad (3.1)$$

The problem domain is confined to the region between the planes $x=0$ and $x=h$ where the boundary condition $B_x=0$ is imposed.

A Fourier representation of the y -dependence will be used, the transformation being written

$$\tilde{W}(x, v, z) = \int_{-\infty}^{\infty} W(x, y, z) e^{-jvy} dy, \quad (3.2)$$

with a corresponding inverse

$$W(x, y, z) = \frac{1}{2\pi} \int_{-\infty}^{\infty} \tilde{W}(x, v, z) e^{jvy} dv. \quad (3.3)$$

The TE potential satisfies the Laplace equation in the domain of the filament problem excluding the filament region and hence its Fourier transform with respect to y is a solution of

$$\left(\frac{\partial^2}{\partial x^2} + \frac{\partial^2}{\partial z^2} - v^2 \right) \tilde{W} = 0. \quad (3.4)$$

The x -dependence of $\partial \tilde{W}_a^{(0)}/\partial x$ is expressed as a Fourier cosine series allowing the solution for a filament in the plane $z=z_0$ to be represented as

$$\frac{\partial \tilde{W}_a^{(0)}}{\partial x} = \mp \left[e^{-v|z-z_0|} A_0^{(0)} + \sum_{i=1}^{\infty} \cos(u_i x) e^{-\kappa_i |z-z_0|} A_i^{(0)} \right], \quad (3.5)$$

where $\kappa_i = \sqrt{u_i^2 + v^2}$ and $\mp = \text{sign}(z_0 - z)$. This form ensures that \tilde{B}_z is continuous in the plane $z=z_0$ as can be verified by taking the derivative of equation (3.5) with respect to z . By putting $u_i = i\pi/h$ the boundary condition $\tilde{B}_x = 0$ is satisfied at $x=0$ and $x=h$, as can be seen from the derivative of equation (3.5) with respect to x . The coefficients in the expansion are determined from the current density in the plane $z=z_0$ written in the general form $\mathbf{J}(x, y)\delta(z-z_0)$. From Ampère's law, it can be shown that the magnetic flux density has a discontinuity in the plane of the source such that

$$\tilde{B}_y^+ - \tilde{B}_y^- = -\mu_0 \tilde{J}_x, \quad (3.6)$$

where \tilde{J}_x is the Fourier transform with respect to the y of the x -component of $\mathbf{J}(x, y)$ and the \pm superscript refers to limiting points above and below the plane $z=z_0$, respectively. Combining equation (3.5) with (3.6), multiplying by $\cos(u_m x)$, $m=0, 1, 2 \dots$ and integrating between 0 and h gives

$$2jvhA_0^{(0)} = \mu_0 \int_0^h \tilde{J}_x(x, v) dx \quad (3.7)$$

and

$$jvhA_m^{(0)} = \mu_0 \int_0^h \cos(u_m x) \tilde{J}_x(x, v) dx, \quad (3.8)$$

where the orthogonality relationship

$$\int_0^h \cos(u_m x) \cos(u_n x) dx = \frac{h}{2} \delta_{mn}, \quad (3.9)$$

has been used. Note that equations (3.7) and (3.8) can be written as

$$2jvhA_0^{(0)} = \mu_0 \int_0^h \int_{-\infty}^{\infty} J_x(x, v) e^{-jvy} dx dy \quad (3.10)$$

and

$$jvhA_m^{(0)} = \mu_0 \int_0^h \int_{-\infty}^{\infty} \cos(u_m x) J_x(x, v) e^{-jvy} dx dy. \quad (3.11)$$

Changing to cylindrical polar coordinates:

$$\left. \begin{aligned} x &= d + r \cos \phi, & y &= r \sin \phi, \\ u_i &= \kappa_i \cos \beta, & v &= \kappa_i \sin \beta, \end{aligned} \right\} \quad (3.12)$$

putting $J_x = -I\delta(r-r_0)\sin \phi$ in equations (3.10) and (3.11) to represent the x -component of the filament current and integrating gives

$$A_i^{(0)} = \epsilon_i \pi \mu_0 I \frac{r_0}{h \kappa_i} \cos(u_i d) J_1(\kappa_i r_0), \quad i = 0, 1, 2 \dots, \quad (3.13)$$

where ϵ_i is the Neumann factor: $\epsilon_0 = 1$ and $\epsilon_i = 2$, $i > 0$. Note that the same result is found using the complementary interface condition

$$\tilde{B}_x^+ - \tilde{B}_x^- = -\mu_0 \tilde{J}_y. \quad (3.14)$$

Substituting for the $A_i^{(0)}$ into equation (3.5) gives

$$\frac{\partial \tilde{W}_a^{(0)}}{\partial x} = \mp \pi \mu_0 I \frac{r_0}{h} \left[\frac{1}{v} J_1(vr_0) e^{-v|z-z_0|} + 2 \sum_{i=1}^{\infty} \frac{1}{\kappa_i} \cos(u_i d) J_1(\kappa_i r_0) \cos(u_i x) e^{-\kappa_i |z-z_0|} \right], \quad (3.15)$$

for the filament potential.

(b) *Coil with a rectangular cross-section*

For a uniformly wound coil of rectangular cross-section having N turns, the x -derivative of the TE potential, found from equation (3.15) by superposition is written

$$\begin{aligned} \frac{\partial \tilde{W}_a^{(0)}}{\partial x} = \pi \mu_0 I \frac{N}{h(r_2 - r_1)(z_2 - z_1)} & \left[\frac{1}{v^4} \chi(vr_1, vr_2) F(vz, vz_1, vz_2) \right. \\ & \left. + 2 \sum_{i=1}^{\infty} \frac{1}{\kappa_i^4} \cos(u_i d) \chi(\kappa_i r_1, \kappa_i r_2) \cos(u_i x) F(\kappa_i z, \kappa_i z_1, \kappa_i z_2) \right], \end{aligned} \quad (3.16)$$

where z_1 and z_2 are the z co-ordinates of the lower and upper surfaces of the coil, respectively. The coil inner radius is r_1 and the outer radius r_2 . The z -dependence of the TE potential for a circular coil is given by

$$F(z, z_1, z_2) = \begin{cases} -e^{-z}(e^{z_2} - e^{z_1}), & z \geq z_2, \\ e^{-(z-z_1)} - e^{-(z_2-z)}, & z_2 \geq z \geq z_1, \\ e^z(e^{-z_1} - e^{-z_2}), & z \leq z_1, \end{cases} \quad (3.17)$$

and we have defined

$$\chi(a_1, a_2) = \int_{a_1}^{a_2} J_1(r) r \, dr, \quad (3.18)$$

which can be expressed in terms of standard functions. For computation purposes, $\chi(a_1, a_2)$ can be expressed in terms of a Meijer G-function or in terms of Struve and Bessel functions (Gradshteyn & Ryzhik 1980). In the quarter space problem, it is convenient to write the x -derivative of the Fourier transformed potential representing the field in the region immediately below the coil ($0 \leq z \leq z_1$; figure 1) as

$$\frac{\partial \tilde{W}_a^{(0)}}{\partial x} = e^{vz} C_0^{(0)} + \sum_{i=1}^{\infty} \cos(u_i x) e^{\kappa_i z} C_i^{(0)}. \quad (3.19)$$

With reference to equations (3.16) and (3.17), the coefficients are given by

$$C_i^{(0)} = \epsilon_i \pi \mu_0 I \frac{N}{h(r_2 - r_1)(z_2 - z_1)} \frac{1}{\kappa_i^4} \cos(u_i d) \chi(\kappa_i r_1, \kappa_i r_2) (e^{-\kappa_i z_1} - e^{-\kappa_i z_2}). \quad (3.20)$$

4. Quarter-space conductor

Consider a conductive quarter space excited by a uniformly wound circular coil of rectangular cross-section carrying alternating current. The conductor fills the region $z < 0$, $0 < x < c$, [figure 1](#) and the coil, located in the half-space $z > 0$, has its axis in the z -direction. In this section we derive the quasi-static magnetic flux density in terms of TE and TM potentials and in §5 give an expression for the coil impedance due to induced current in the conductor. This can be accomplished for the quasi-static limit without defining the TM potential in air or the conservative part of the electric field in air, by using the continuity of the normal magnetic flux and tangential magnetic field at conductor–air interfaces.

As a guide to the application of the interface conditions, the following expressions for the magnetic flux density are given here for reference:

$$\mathbf{B} = \nabla \times \nabla \times (\hat{x} W_a) + k^2 \nabla \times (\hat{x} W_b), \quad (4.1)$$

where $k^2 = j\omega\mu\sigma$. Components of the magnetic flux density are therefore

$$B_x = \frac{\partial^2 W_a}{\partial x^2} - k^2 W_a, \quad B_y = \frac{\partial^2 W_a}{\partial x \partial y} + k^2 \frac{\partial W_b}{\partial z}, \quad B_z = \frac{\partial^2 W_a}{\partial x \partial z} - k^2 \frac{\partial W_b}{\partial y}. \quad (4.2)$$

For the non-conductive regions, the terms containing k^2 vanish and \mathbf{B} can be written as in equation (3.1).

(a) Transverse electric potential

The positive z half-space is designated region 1 and the negative z half-space as region 2. Coefficients in the series representations of the magnetic field in these regions are correspondingly given superscripts (1) and (2) whereas the superscript (0) refers to the prescribed whole domain coil solution defined in §3. The Fourier transform with respect to y of the TE potential satisfies equation (3.4) in region 1 except at the source coil. The solution for the region above the plane $z=0$ but below the coil ($0 \leq z \leq z_1$; [figure 1](#)), is written $\tilde{W}_a^{(0)} + \tilde{W}_a^{(1)}$ where $\tilde{W}_a^{(0)}$ is given by equations (3.19) and (3.20). For $0 \leq z \leq z_1$, we write the potential due to eddy currents in the conductor as

$$\frac{\partial \tilde{W}_a^{(1)}}{\partial x} = e^{-vz} C_0^{(1)} + \sum_{i=1}^{\infty} \cos(u_i x) e^{-\kappa_i z} C_i^{(1)}. \quad (4.3)$$

To ensure that the x -component of the magnetic flux at the boundary $x=h$ is zero, we retain the discrete values $u_i = i\pi/h$. Again, the correct z -dependence requires that $\kappa_i = \sqrt{u_i^2 + v^2}$, where the positive root is taken.

For the non-conductive region below the $z=0$ plane, the TE potential satisfies equation (3.4). For the conductive region below this plane, however, the TE potential satisfies

$$\left[\frac{\partial^2}{\partial x^2} + \frac{\partial^2}{\partial z^2} - (v^2 + k^2) \right] \tilde{W} = 0. \quad (4.4)$$

The TE solution for the lower half space ($z < 0$) has the form

$$\frac{\partial \tilde{W}_a^{(2)}}{\partial x} = \begin{cases} \sum_{i=1}^{\infty} \cos(q_i x) e^{\gamma_i z} C_i^{(2)}, & 0 \leq x < c, \\ e^{vz} C_0^{(2)} + \sum_{i=1}^{\infty} \cos[p_i(h-x)] e^{\gamma_i z} \alpha_i C_i^{(2)}, & c \leq x < h, \end{cases} \quad (4.5)$$

where $p_i = \sqrt{q_i^2 + k^2}$ and $\gamma_i = \sqrt{q_i^2 + v^2 + k^2}$.

The cosine series representation potentially includes a term $\exp(\sqrt{v^2 + k^2}z)$ in the expression (4.5), for the region $0 \leq x \leq c$, but this additional term vanishes when the continuity of B_x is enforced across the interface $x = c$. The solution for the non-conductive region $c \leq x < h$ below the $z=0$ plane is written in equation (4.5) with a z -dependence $\exp(\sqrt{q_i^2 + v^2 + k^2}z)$ to match that for the field in the conductor. Then the x -dependence for $c \leq x < h$ below $z=0$, is written with a modified eigenvalue $p_i = \sqrt{q_i^2 + k^2}$ so that the expression for the TE potential satisfies equation (3.4). As a consequence, coupling across the $x=c$ interface takes effect on a term-by-term basis, each eigenfunction for the conductive region being matched by one for the air region having the same z -dependence.

The continuity of B_x and H_y at the $x=c$ interface implies that

$$p_i \sin(q_i c) = -\alpha_i q_i \sin[p_i(h-c)] \quad (4.6)$$

and

$$\cos(q_i c) = \alpha_i \cos[p_i(h-c)], \quad (4.7)$$

respectively. Combining these gives

$$\sqrt{q_i^2 + k^2} \tan(q_i c) + q_i \tan[\sqrt{q_i^2 + k^2}(h-c)] = 0, \quad (4.8)$$

from which the eigenvalues q_i are found, and subsequently, α_i determined from equation (4.7). Note that the eigenvalues are independent of v and are calculated once for a given h and c and a fixed k^2 .

(b) Transverse magnetic potential

The TM potential, like the TE potential for the conductive region, satisfies equation (4.4), the solution being of the form $\cos(r_i x) e^{s_i z}$, where s_i is the root of $s_i^2 = r_i^2 + v^2 + k^2$ with a positive real part. At the interface $x=c$, the normal component of the electric current density, $-j\omega\sigma\nabla \times \nabla \times (\hat{x}W_b)$, is zero. This implies that the function $W_b(c, y, z)$ satisfies a two-dimensional Laplace equation and that

$$\left(\frac{\partial^2}{\partial z^2} - v^2 \right) \tilde{W}_b(c, v, z) = 0. \quad (4.9)$$

Since the solution of equation (4.4) is of the form $\cos(r_i x) e^{s_i z}$, the boundary condition (4.9) is satisfied by letting $(r_i^2 + k^2)\cos(r_i c) e^{s_i z} = 0$, which implies that the required eigenvalues are $r_0 = \pm jk$ and $r_i = (i - \frac{1}{2})\pi/c$, $i = 1, 2, 3 \dots$. It follows that the TM potential can be written

$$k^2 \tilde{W}_b = \cosh(kx) e^{vz} D_0 + \sum_{i=1}^{\infty} \cos(r_i x) e^{s_i z} D_i. \quad (4.10)$$

The complex eigenvalue r_0 giving rise to the hyperbolic cosine term is due to the wedge and does not appear in the half-space solution. It was also taken into account by Flitz & Nethe (1993) where a problem of eddy current induction in a finite length cylinder was studied.

Note that from equations (4.5), (4.10) and the continuity of H_y at $x=c$, it is found that

$$C_0^{(2)} = -j \cosh(kc)D_0. \quad (4.11)$$

We next consider the evaluation of the remaining coefficients, $C_i^{(1)}$, $C_0^{(1)}$, $C_i^{(2)}$, D_i and D_0 ($i=1, 2, 3 \dots$) via the continuity conditions that apply to the tangential magnetic field and normal magnetic flux at the plane $z=0$.

(c) *Magnetic field and flux continuity*

The continuity conditions on the magnetic field are satisfied at the plane $z=0$ by applying the orthogonality properties of the sine and cosine functions to determine the relationship between Fourier coefficients. Specifically, one equates expressions for the field components which are then multiplied by $\cos(u_i x)$ for the y and z components and by $\sin(u_i x)$ in the case of the x -component; then integrated between 0 and h . First this procedure is carried out using the continuity of H_y and B_z for $u_i=0$ leading to the relationships

$$\int_0^h \tilde{H}_y^{(0)} + \tilde{H}_y^{(1)} dx = \int_0^h \tilde{H}_y^{(2)} dx$$

and

$$\int_0^h \tilde{B}_z^{(0)} + \tilde{B}_z^{(1)} dx = \int_0^h \tilde{B}_z^{(2)} dx.$$

With reference to the field components, equation (4.2), and the general expressions for the TE and TM potentials, (4.3), (4.5) and (4.10), it is found that

$$jvh(C_0^{(0)} + C_0^{(1)}) = \frac{v}{k} [\sinh(kc) + k(h-c)\cosh(kc)]D_0 + \sum_{i=1}^{\infty} (-1)^{i+1} \frac{s_i}{r_i} D_i \quad (4.12)$$

and

$$jvh(C_0^{(0)} - C_0^{(1)}) = \frac{v}{k} [\sinh(kc) + k(h-c)\cosh(kc)]D_0 + \sum_{i=1}^{\infty} (-1)^{i+1} \frac{v}{r_i} D_i, \quad (4.13)$$

where equation (4.11) has been used. Solving for $C_0^{(1)}$ and D_0 gives

$$C_0^{(1)} = \mathbf{R}_-^T \mathbf{D} \quad (4.14)$$

and

$$D_0 = \lambda(C_0^{(0)} - \mathbf{R}_+^T \mathbf{D}), \quad (4.15)$$

where

$$\lambda = \frac{jhk}{[\sinh(kc) + k(h-c)\cosh(kc)]}. \quad (4.16)$$

Column vectors, \mathbf{R}_{\pm} , whose components are

$$R_{\pm, i} = \frac{1}{j2vh} (-1)^{i+1} \frac{s_i \pm v}{r_i} \quad (4.17)$$

have been introduced, \mathbf{D} is a column vector of the expansion coefficients D_i , $i=1, 2, 3 \dots$, and superscript T denotes the transpose of the vector.

Next, we seek to ensure that the tangential magnetic field is continuous at $z=0$ through the relationships

$$\int_0^h \sin(u_i x) [\tilde{H}_x^{(0)} + \tilde{H}_x^{(1)}] dx = \int_0^h \sin(u_i x) \tilde{H}_x^{(2)} dx \quad (4.18)$$

and

$$\int_0^h \cos(u_i x) [\tilde{H}_y^{(0)} + \tilde{H}_y^{(1)}] dx = \int_0^h \cos(u_i x) \tilde{H}_y^{(2)} dx, \quad (4.19)$$

with $i=1, 2, 3 \dots$. Also the continuity of normal flux density is sought through the equation

$$\int_0^h \cos(u_i x) [\tilde{B}_z^{(0)} + \tilde{B}_z^{(1)}] dx = \int_0^h \cos(u_i x) \tilde{B}_z^{(2)} dx. \quad (4.20)$$

The continuity conditions at $z=0$ give rise to relationships that are expressed in matrix form

$$\mathbf{u}(\mathbf{C}^{(0)} + \mathbf{C}^{(1)}) = \mathbf{M}_s \mathbf{p} \mathbf{C}^{(2)}, \quad (4.21)$$

$$jv(\mathbf{C}^{(0)} + \mathbf{C}^{(1)}) = jv\mathbf{M}_c \mathbf{C}^{(2)} + v\mathbf{L}D_0 + \mathbf{M}_r \mathbf{s} \mathbf{D}, \quad (4.22)$$

and

$$\boldsymbol{\kappa}(\mathbf{C}^{(0)} - \mathbf{C}^{(1)}) = \mathbf{M}_c \boldsymbol{\gamma} \mathbf{C}^{(2)} - jv\mathbf{L}D_0 - jv\mathbf{M}_r \mathbf{D}, \quad (4.23)$$

where \mathbf{u} , \mathbf{p} and \mathbf{s} are diagonal matrices with diagonal elements u_i , p_i and s_i , respectively. $\mathbf{C}^{(0)}$, $\mathbf{C}^{(1)}$, $\mathbf{C}^{(2)}$ and \mathbf{D} are column vectors of the expansion coefficients; and \mathbf{M}_s , \mathbf{M}_c and \mathbf{M}_r are matrices defined in the appendix together with the vector \mathbf{L} . For the impedance calculations, the electromagnetic field in the region $z>0$ is required which means that the solution for $\mathbf{C}^{(1)}$ is sought. Eliminating D_0 using equation (4.15) and $\mathbf{C}^{(2)}$ using equation (4.21) gives the form

$$\left. \begin{aligned} \mathbf{A}_{11} \mathbf{C}^{(1)} + \mathbf{A}_{12} \mathbf{D} &= \mathbf{K}_1 \mathbf{C}^{(0)} + \mathbf{L}_1 C_0^{(0)}, \\ \mathbf{A}_{21} \mathbf{C}^{(1)} + \mathbf{A}_{22} \mathbf{D} &= \mathbf{K}_2 \mathbf{C}^{(0)} + \mathbf{L}_2 C_0^{(0)}. \end{aligned} \right\} \quad (4.24)$$

Note that the matrices \mathbf{A}_{mn} , \mathbf{K}_m and \mathbf{L}_m ($m, n=1, 2$) are used here to show the form of the solution but these are not given explicitly. The solution can be written

$$\mathbf{C}^{(1)} = \mathbf{M} \mathbf{C}^{(0)} + \mathbf{V} C_0^{(0)}, \quad (4.25)$$

with

$$\mathbf{M} = (\mathbf{A}_{11} - \mathbf{A}_{12} \mathbf{A}_{22}^{-1} \mathbf{A}_{21})^{-1} (\mathbf{K}_1 - \mathbf{A}_{12} \mathbf{A}_{22}^{-1} \mathbf{K}_2), \quad (4.26)$$

$$\mathbf{V} = (\mathbf{A}_{11} - \mathbf{A}_{12} \mathbf{A}_{22}^{-1} \mathbf{A}_{21})^{-1} (\mathbf{L}_1 - \mathbf{A}_{12} \mathbf{A}_{22}^{-1} \mathbf{L}_2), \quad (4.27)$$

and

$$\mathbf{D} = \mathbf{A}_{12}^{-1}(-\mathbf{A}_{11}\mathbf{C}^{(1)} + \mathbf{K}_1\mathbf{C}^{(0)} + \mathbf{L}_1\mathbf{C}_0^{(0)}). \quad (4.28)$$

Using equation (4.25) together with equations (3.19), (3.20) and (4.3), the field for $z > 0$ can be found. A similar procedure gives the field for $z < 0$.

5. Impedance

The impedance change due to the presence of induced current in a conductor is derived by calculating the rate of change of flux linkage to the coil from the z -component of magnetic flux density due to eddy currents

$$\Delta B_z = -\frac{1}{2\pi} \int_{-\infty}^{\infty} \left[ve^{-vz} C_0^{(1)} + \sum_{i=1}^{\infty} \cos(u_i x) \kappa_i e^{-\kappa_i z} C_i^{(1)} \right] e^{jvy} dv, \quad (5.1)$$

where the z -derivative of the appropriate terms from equation (4.3) have been used. The induced emf in a single circular filament of radius r_0 at $z = z_0$ is given by

$$\Delta V(r_0, z_0) = -j2\pi\omega \int_0^{r_0} \Delta B_z(r, z_0) r dr. \quad (5.2)$$

Integrating with respect to r_0 and z_0 over the coil cross-section gives

$$\begin{aligned} I\Delta Z = & -\frac{j2\pi\omega N}{(r_2 - r_1)(z_2 - z_1)} \left[\int_{-\infty}^{\infty} \frac{(e^{-vz_1} - e^{-vz_2})}{v^3} \chi(vr_1, vr_2) C_0^{(1)} dv \right. \\ & \left. + \int_{-\infty}^{\infty} \sum_{i=1}^{\infty} \frac{(e^{-\kappa_i z_1} - e^{-\kappa_i z_2})}{\kappa_i^3} \cos(u_i d) \chi(\kappa_i r_1, \kappa_i r_2) C_i^{(1)} dv \right], \end{aligned} \quad (5.3)$$

where $C_i^{(1)}$ is given by equations (4.14) and (4.25). For a half-space conductor, it is found by letting $c = h$ that

$$C_i^{(1)} = \frac{\gamma_i - \kappa_i}{\gamma_i + \kappa_i} C_i^{(0)} \quad i = 0 \dots \infty. \quad (5.4)$$

By using equation (3.20) in (5.3), it is found that

$$I^2 \Delta Z = -\frac{j2\omega h}{\mu_0} \sum_{i=0}^{\infty} \frac{1}{\epsilon_i} \left[\int_{-\infty}^{\infty} C_i^{(0)} C_i^{(1)} \kappa_i dv \right]. \quad (5.5)$$

Because both $C_i^{(0)}$ and $C_i^{(1)}$ are proportional to the current density in the coil, it can be seen that the impedance is proportional to the square of the turns density.

6. Corroboration

The validity of equation (5.3) has been tested by comparing numerical calculations to experiment. Firstly, the numerical performance of the impedance calculations were examined by calculating the change in coil impedance due to a half-space conductor using equations (5.3) with (5.4). Calculations were carried

Table 1. *Coil impedance change (Ω) due to half-space*

	coil C5	coil C27
experiment	22.0 $-j$ 70.5	12.65 $-j$ 125.1
Dodd & Deeds (1968)	22.20 $-j$ 70.49	12.801 $-j$ 125.388
equation (5.3)	22.25 $-j$ 70.45	12.801 $-j$ 125.329

Table 2. *Coil parameters*

parameter	coil C5	coil C27
r_1 (mm)	9.33	7.04
r_2 (mm)	18.04	12.4
z_1 (mm)	3.32	3.43
z_2 (mm)	13.37	8.47
N	1910	556

Table 3. *Conductive block parameters*

parameter	block B1	block B2
ρ ($\mu\Omega$ cm)	3.92	4.58
thickness (mm)	140	65

out using MATHEMATICA. The integral was computed with Gauss–Legendre integration after truncating at $v = \pm 10/r_2$, while for the summation, 100 terms were used with $h = 20r_2$. The latter method was the one used also in the case of the conductive quarter-space. The complex eigenvalues were computed with the MATHEMATICA routine FindRoot. The three matrix inversions, needed in the calculations, were done with the MATHEMATICA routine Inverse, which uses LU (lower triangular and upper triangular) decomposition.

Numerical calculations for the half-space conductor were compared to an integral formula (Dodd & Deeds 1968), which was evaluated using an automatic integration routine (DQDAGI from Fortran IMSL Libraries) thus providing an accurate result. The results, shown in table 1, were obtained based on the coil parameters in table 2 and conductive block parameters in table 3. The agreement between the two theoretical results gives confidence in the numerical approach for computing the coil impedance variation (5.3) in the case of a quarter-space.

The experimental data for validating coil impedance variations in the presence of a conductive quarter space consists of two measurement sets provided by Burke & Ibrahim (2004). The first is for coil C5 at 850 Hz and the second is for coil C27 operated at 20 kHz. Impedance change measurements were recorded as a function of position, at 2 mm intervals, while the coils were moved across the edges of thick aluminium alloy blocks. The coil position referred to in figures 3–6

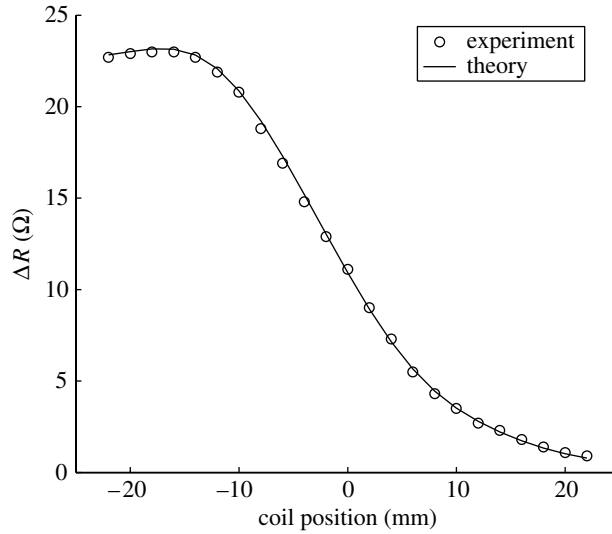


Figure 3. Resistance variation with coil axis position relative to the edge of the conductor B1 for coil C5 excited at 850 Hz.

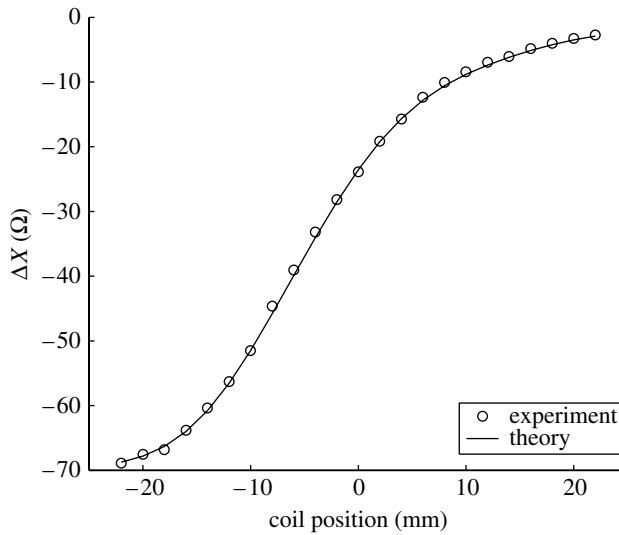


Figure 4. Reactance variation with coil axis position relative to the edge of the conductor B1 for coil C5 excited at 850 Hz.

is the distance between the coil's axis position and the edge, $d - c$, and it is zero when the coil centre is directly above the edge.

The conductive block data are listed in [table 3](#). The C5 coil was used with block B1 which has a thickness 7.8 times the coil radius. The C27 coil was used with block B2 which has a thickness 5.2 times the coil radius. Initially the C5 coil was also used with the 65 mm thick aluminium alloy block but a small disagreement between theory and experiment was noticed. It was conjectured

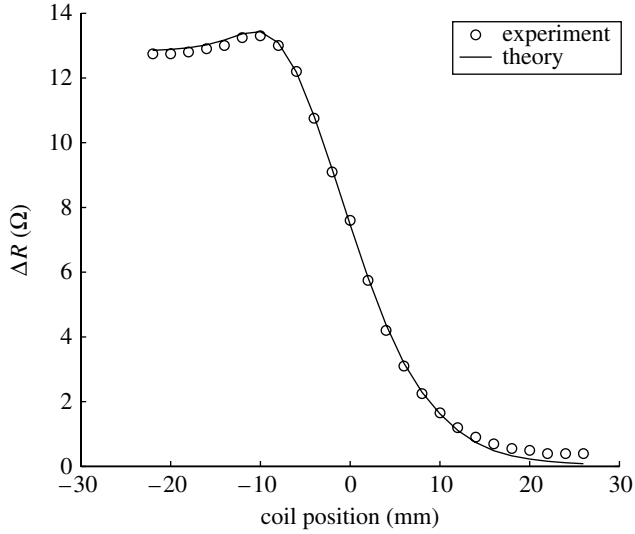


Figure 5. Resistance variation with coil axis position relative to the edge of the conductor B2 for coil C27 excited at 20 kHz.

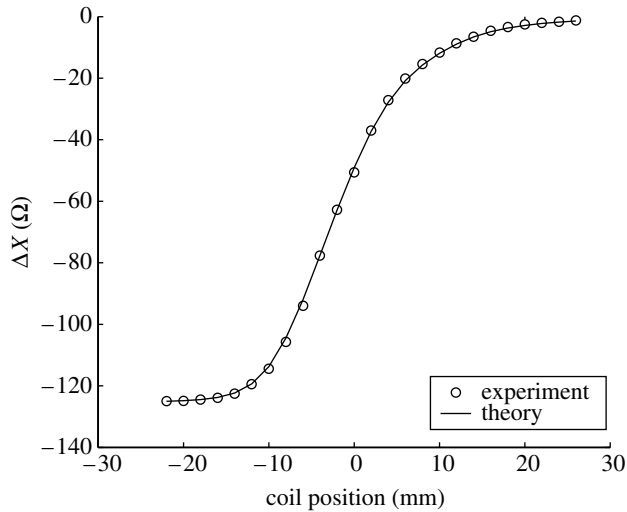


Figure 6. Reactance variation with coil axis position relative to the edge of the conductor B2 for coil C27 excited at 20 kHz.

that this block did not provide an accurate approximation of a quarter-space when used in conjunction with the large C5 coil. The use of the thicker 140 mm block and the corresponding improvement in agreement supported the conjecture.

The results cover cases where the skin depth is both small (0.762 mm at 20 kHz) and relatively large (3.418 mm at 0.85 kHz). The agreement between predictions and experiment is very good in both cases, the difference being roughly 1%, figures 3–6. A significant feature of these results is that while the coil

reactance increases monotonically as the coil is traversed across the edge of the conductive block, the resistance peaks before decreasing. This is a characteristic edge effect noted also in tube testing (Theodoulidis 2004).

7. Conclusion

The quasi-static magnetic field of a coil carrying an alternating current in the presence of a conductive right-angled corner conductor has been calculated using the TREE method, explained here. The coil impedance change due to eddy currents in the conductor has also been determined allowing a comparison of the coil impedance variations with experiments in which the coil is moved over the edge of the conductor. The results show good agreement with experiment both at low frequencies and at a frequency where the skin depth is small compared with the coil diameter.

The solution can be extended to the case of a plate with the coil moving across its edge and to geometries involving planar conductors with long cracks or slots. Work is underway for deriving solutions to these canonical problems as well as for applying the TREE method to three-dimensional eddy current NDE problems described in cylindrical coordinates.

The authors would like to thank Steve Burke and Matthew Ibrahim of DSTO Melbourne for providing experimental data. The work of J.R.B. was performed with the support of the National Science Foundation/Industry University Cooperative Research Consortium at the Center for Nondestructive Evaluation and that of T.P.T. with funding from the Air Force Research Laboratory through S&K Technologies, Inc. on delivery order number 5007-IOWA-001 of the prime contract F09650-00-D-0018.

Appendix A. Matrix definitions

This appendix defines the matrices and vectors used in forming equations (4.21)–(4.23). The matrix \mathbf{M}_s , equation (4.21), is derived from the right-hand side of the continuity condition (4.18) for H_x at the $z=0$ interface with the x -component of the field deduced from (4.5). Thus

$$\mathbf{M}_{s,ij} = \frac{2}{h} \left\{ \frac{p_j}{q_j} \int_0^c \sin(u_i x) \sin(q_j x) dx - \alpha_j \int_c^h \sin(u_i x) \sin[p_j(h-x)] dx \right\}, \quad (\text{A } 1)$$

where α_j is given by equation (4.7). This can be written

$$\mathbf{M}_{s,ij} = \frac{p_j}{q_j} \mathbf{M}_{s,ij}^{(1)} - \alpha_j \mathbf{M}_{s,ij}^{(2)}, \quad (\text{A } 2)$$

where

$$\mathbf{M}_{s,ij}^{(1)} = \begin{cases} \frac{\sin[c(q_j - u_i)]}{h(q_j - u_i)} - \frac{\sin[c(q_j + u_i)]}{h(q_j + u_i)} & \text{for } q_j \neq u_i, \\ \frac{c}{h} - \frac{\sin 2cu_i}{2hu_i} & \text{for } q_j = u_i, \end{cases} \quad (\text{A } 3)$$

and

$$M_{s,ij}^{(2)} = \begin{cases} \frac{1}{h} \left\{ \frac{\sin[(h-c)(p_j+u_j)]}{p_j+u_j} - \frac{\sin[(h-c)(p_j-u_j)]}{p_j-u_j} \right\} \cos(hu_i) & \text{for } p_j \neq u_i, \\ \frac{1}{h} \left\{ \frac{\sin[2(h-c)u_i]}{2u_i} - (h-c) \right\} \cos(hu_i) & \text{for } p_j = u_i. \end{cases} \quad (\text{A } 4)$$

Similarly, from the right-hand side of equations (4.5) and (4.19) we get

$$M_{c,ij} = \frac{2}{h} \left\{ \int_0^c \cos(u_i x) \cos(q_j x) dx + \alpha_j \int_c^h \cos(u_i x) \cos[p_j(h-x)] dx \right\}. \quad (\text{A } 5)$$

This can be written

$$M_{c,ij} = M_{c,ij}^{(1)} + \alpha_j M_{c,ij}^{(2)}, \quad (\text{A } 6)$$

where

$$M_{c,ij}^{(1)} = \begin{cases} \frac{\sin[c(q_j-u_i)]}{h(q_j-u_i)} + \frac{\sin[c(q_j+u_i)]}{h(q_j+u_i)} & \text{for } q_j \neq u_i, \\ \frac{c}{h} + \frac{\sin 2cu_i}{2hu_i} & \text{for } q_j = u_i, \end{cases} \quad (\text{A } 7)$$

and

$$M_{c,ij}^{(2)} = \begin{cases} \frac{1}{h} \left\{ \frac{\sin[(h-c)(p_j+u_j)]}{p_j+u_j} + \frac{\sin[(h-c)(p_j-u_j)]}{p_j-u_j} \right\} \cos(hu_i) & \text{for } p_j \neq u_i, \\ \frac{1}{h} \left\{ \frac{\sin[2(h-c)u_i]}{2u_i} + (h-c) \right\} \cos(hu_i) & \text{for } p_j = u_i. \end{cases} \quad (\text{A } 8)$$

From equations (4.10) and (4.19) we get equation (4.22) where

$$M_{r,ij} = \frac{2}{h} \int_0^c \cos(u_i x) \cos(r_j x) dx = \begin{cases} \frac{\sin[c(r_j-u_i)]}{h(r_j-u_i)} + \frac{\sin[c(r_j+u_i)]}{h(r_j+u_i)} & \text{for } r_j \neq u_i, \\ \frac{c}{h} + \frac{\sin 2cu_i}{2hu_i} & \text{for } r_j = u_i, \end{cases} \quad (\text{A } 9)$$

and

$$L_i = \frac{2}{h} \left\{ \int_0^c \cosh(kx) \cos(u_i x) dx + \cosh(kc) \int_c^h \cos(u_i x) dx \right\} = \frac{2k[u_i \cos(cu_i) \sinh(ck) - k \cosh(ck) \sin(cu_i)]}{u_i h(k^2 + u_i^2)}. \quad (\text{A } 10)$$

References

- Budaev, B. 1995 *Diffraction by wedges*. New York: Wiley.
- Burke, S. K. & Ibrahim, M. 2004 Feb 3D edge effect in eddy-current NDE: experimental data for a cylindrical air-cored coil and an Al alloy quarter space. DSTO, Melbourne.
- Dodd, C. V. & Deeds, W. E. 1968 Analytical solutions to eddy-current probe-coil problems. *J. Appl. Phys.* **39**, 2829–2838.
- Flitz, M. & Nethe, A. 1993 Bemerkungen zur losung des dreidimensional wirbelstromproblems in kreiszylindern endlicher lange. *Arch. Elektrotech.* **76**, 195–200.
- Gradshteyn, I. S. & Ryzhik, I. M. 1980 *Tables of integrals, series and products, 6.561, 5th edn., p. 707*. New York: Academic Press.
- Rawlins, A. D. 1999 Diffraction by, or diffusion into, a penetrable wedge. *Proc. R. Soc. A* **455**, 2655–2686.
- Tai, C. C., Yang, H.-C. & Liu, Y.-H. 2002 Modelling the surface condition of ferromagnetic metal by the swept frequency eddy-current method. *IEEE Trans. Magn.* **38**, 205–210.
- Theodoulidis, T. P. 2003 Model of ferrite-cored probes for eddy current nondestructive evaluation. *J. Appl. Phys.* **93**, 3071–3078.
- Theodoulidis, T. P. 2004 End effect modelling in eddy current tube testing with bobbin coils. *Int. J. Appl. Electromag. Mech.* **19**, 207–212.